The International Journal of Advanced Manufacturing Technology (2026) 142:3699–3718
https://doi.org/10.1007/s00170-025-17125-y

ORIGINAL ARTICLE

Ploughing and shearing machining mechanisms in ball-end milling of free-form surfaces

Rodrigo Voigt[1] · Felipe Marin[1,4] · Igor Fernando Basso[2] · Alexandre Mikowski[1] · Alessandro Roger Rodrigues[3] · Fabio Antonio Xavier[4] · Adriano Fagali de Souza[4]

Received: 6 November 2025 / Accepted: 25 November 2025 / Published online: 10 January 2026

Abstract
The current research investigated the influences of tool surface engagement (TSE), material hardness, and cutting parameters on the machining force and roughness when milling free-form surfaces with a ball-end cutting tool. The frequent alteration of the TSE (as typically encountered in this milling process) also alters the dominant cutting mechanism, either ploughing or shearing. The phenomena occurring in such machining processes are still not fully understood, and their comprehension is fundamental for the development of any robust model to predict such processes. Machining experiments were conducted by varying the TSE (angle φ) and workpiece hardness (AISI H13 steel: annealed 227 HV and hardened 495 HV). A geometric study allows identifying a critical geometric cutting condition - the ξ angle, which corresponds to the angle of chip extension. It is driven by the cutting parameters together with the TSE. The ξ angle allows identifying the cutting condition in terms of force and roughness. When the ξ angle is altered, the predominance of the machining mechanism is also altered between ploughing and shearing. Thus, a new specific Ks coefficient according to ξ angle was established, $Ks_{(\varphi)}$ and $Ks_{(\xi)}$, to estimate the machining force according to the tool position along the trajectory. The ξ angle, together with material hardness, allowed the identification of distinct surface damage patterns that affect the surface roughness Sz.

Keywords Ball-end milling · Effective cutting speed · Surface roughness · Ploughing · Machining force

1 Introduction

Free-form surfaces have been used over the last decades in automotive, aeronautical, medical, and other industries to meet aesthetic and functional demands [1]. Milling with a ball-end cutting tool is the most used process for machining such surfaces [2]. In contrast to ordinary milling, the tool surface engagement (TSE) alters constantly along the toolpath when milling a free-form surface. These TSE alterations and the process parameters directly influence the surface roughness of the machined component [3]. Besides, they are associated with the intermittent cutting condition that affects the machining force, tool wear, form deviations and vibrations [4].

In such a milling process, the TSE shifts the dominant material removal mechanism from ploughing (plastic deformation) to shearing [5, 6], which makes the process highly dependent on geometry, workpiece material, and toolpath planning. These factors increase process complexity and result in varied surface finishes [7]. The ordinary theoretical surface (which considers only geometric aspects of the process) cannot properly represent the surface texture and roughness in most cases, and it still lacks a better comprehension of the relationships among the TSE, cutting parameters and material properties [8].

Feng et al. [9] analytically investigated the milling texture, and the comparison with experimental results shows that elastic recovery takes place, resulting in several deviations from the theoretical surface. Besides, it was observed

✉ Adriano Fagali de Souza
adriano.fagali@ufsc.br

[1] Department of Mobility Engineering, Federal University of Santa Catarina (UFSC), Joinville, Brazil

[2] Federal Technological University of Paraná, Medianeira, Brazil

[3] University of São Paulo (USP), São Carlos, Brazil

[4] Department of Mechanical Engineering, Federal University of Santa Catarina (UFSC), Florianópolis, Brazil

that as the feed rate increases, the associated errors in the surface topography also increase. One possible cause may be related to recrystallisation effects during machining, which modify material properties associated with grain-size-dependent parameters, as described in the Johnson–Cook model [10].

Marin et al. [11], evaluating ball-end milling of free-form surfaces, modelled the chest height in the feed direction and observed that the surface roughness is influenced by the lead angle. At lead angles close to the tool centre actuation (5° lead angle), the generated surface is dominated by plastic deformation, whereas at higher lead angles, the deviations from the ideal surface are mostly influenced by tool runout. Thus, for a precise determination of roughness, the trochoidal movement of the tool must be considered. This shows that for different materials, the roughness behaviour differs from the theoretical prediction, and that topological inspection and quantification of the surface roughness are good indicators when evaluating the surface texture across a wide range of experiments.

The challenges in quantifying these errors conventionally lead the industry to apply manual polishing to achieve the roughness requirements of free-form surfaces, which can degrade dimensional tolerances [12]. Tolerances for dies and moulds are stringent, ranging from 0.05 to 0.1 mm for stamping and lower than 0.04 mm for injection moulding [13].

These requirements become even more challenging when machining hardened hot-working alloys (30–60 HRC), where increased material hardness can amplify dimensional deviations but also increase the chip brittleness, potentially improving the process window for stable machining. Among them, AISI H13, a Cr-Mo-V alloy steel, is widely used in hot-stamping moulds due to its thermal shock resistance, toughness, and heat stability [14]. When hardened, it retains superior toughness at elevated temperatures [15], which promotes brittle fracture behaviour and improves surface finishing [16]. Also, residual stresses are generated during the heat treatment process, which can cause distortions in previously machined parts. As a result, there is a growing trend towards machining hardened materials.

Prior studies on the ball-end milling of free-form surfaces provide critical insights into optimal tool orientations, toolpaths, and cutting parameters for achieving tight tolerances. Lacalle et al. [17] demonstrated that downward concordant cutting minimises deflection, challenging the linear cantilever assumption. Beyond orientation, error compensation strategies have also been explored. Ma et al. [15] developed an algorithm to modify the NC code to reduce machining errors by considering tool deviations according to the workpiece engagements and machining force, which are governed by tool geometry, workpiece material, cutting conditions, and direction, which also affect the surface texture.

Free-form ball-end milling lacks a universal definition, as the instantaneous surface curvature dynamically affects chip formation [18]. Selecting toolpath strategies (e.g., optimised toolpaths and tilt angles) to minimise forces improves surface finish and reduces deviations [19]. The toolpath strategy influences the force components, geometric error and the tool wear [11]. Multiple studies have demonstrated that surface quality can be improved by minimising the machining force through optimised parameters and toolpaths. It is known that tool trajectories and cutting direction influence the process and the final surface due to the variation in the tool inclination angle [20].

Depending on the process parameters, the direction of tool movement, and the curvature of the surface, the tool tip centre may engage on the surface, causing significant changes in cutting forces and surface quality. When the tool tip's centre acts on the surface, the cutting speed reaches zero, and the material is crushed rather than sheared, affecting thermomechanically the workpiece and the chip formation [21]. This condition can double the machining force, degrading surface finish, particularly in ductile materials [22].

The influences of ploughing and/or shearing mechanisms on cutting force levels remain poorly understood. These effects depend on the TSE and the properties of the material to be machined. In this context, Basso et al. [6] identified three TSE conditions to describe the ball-end milling: (i) tool tip contact with the final surface (Tip-On surface), (ii) tool tip participation in cutting without forming the final surface (Tip-Out surface/Tip-on-chip), and (iii) tool tip disengaged (Tip-Off). Nevertheless, further in-depth investigation into the mapping of tool-surface engagement (TSE) across materials with different properties is still required.

Regarding the cutting strategy, the literature recommends down-milling instead of up-milling for a superior surface finish, because it reduces plastic deformation [23]. Yao et al. [24] showed that transverse down-milling minimises the tool indentation effect, resulting in lower surface roughness in TC17 titanium alloy. However, detrimental effects related to low cutting speeds were observed for ductile materials.

Wu et al. [25] attribute the instability of up-milling to increased tangential force and reduced axial force, which exacerbate vibrations in low-rigidity tools when machining hard materials typically used for moulds and dies. Conversely, Scandiffio et al. [26] reported that when machining hardened AISI D6 (60 HRC), and when the tool tip is engaged in the cutting process, it improved the cutting stability and surface roughness. It happened because a high Fz component, together with the tool tip against the machined surface, assured stiffness during the machining.

Magalhães et al. [27] evaluated the machining of cylindrical specimens of AISI H13 (52 HRC). When the tool tip centre was disengaged, the ascending cut produced a superior surface finish. However, with the tool tip contact, in descending cut, surface roughness (Ra) improved by approximately 100%. Conversely, Souza et al. [28] found that ascending cut yielded lower roughness and forces on AISI P20 (30 HRC), mostly because of a higher effective cutting speed and the avoidance of the tool tip centre. These findings underscore how force behaviour critically varies in ascending and descending cutting.

The effect of the ball-end tool tip on the milled surface and its interaction with materials of different hardness is still not well addressed in the current literature. These factors are important to be considered in a future robust model to predict the machining force, cutting tool wear, geometrical error and roughness of the machined surface, to anticipate potential issues and optimise productivity under such milling conditions [29]. Accordingly, this paper presents a study aimed at achieving a deep understanding of the ball-end milling phenomena, identifying the influence of tool inclination and material properties on machining force and surface results during the milling of free-form geometries.

2 Materials and methods

The present work investigates the influence of material hardness and variations in tool–surface engagement (TSE) on the cutting phenomena, considering the predominance of ploughing and/or shearing cutting mechanisms during the milling of free-form surfaces with a ball-end cutting tool. Machining experiments were carried out alongside a geometrical analysis of the tool–surface engagement, supported by CAD software to correlate the effective cutting tool diameter and effective cutting speed with machining force and surface roughness. Two ball-end tool diameters were evaluated, and AISI H13 steel blocks were used as workpieces under two hardness conditions. The experimental procedures are detailed ahead.

2.1 Workpiece geometry, machining experiments and the evaluations carried out

A quarter-cylindrical geometry was machined longitudinally at different angular positions to represent the distinct tool–surface engagements (TSE) typically encountered in free-form milling. This setup enabled the investigation of this complex machining condition. Seven cutting contact angles (φ) were defined: 0°, 10°, 20°, 30°, 45°, 60°, and 85°. For each angular position, ten passes were executed.

The selection of the angles was based on the variation of the tooltip centre contact. As the slow transition occurs at the tooltip centre and more complex phenomena take place, increments of 10 degrees were selected, extending up to 30°, where the tooltip is no longer in contact with the chip. Afterwards, increments of 15 degrees were used, since the tooltip is no longer in contact and the effective cutting speed dominates the behaviour, up to 60°. Finally, 85° was selected to evaluate a tangential cutting condition, where the spherical dome of the tool is still in cut. Figure 1 illustrates the workpiece and the corresponding toolpaths at the different angular positions, as generated using Siemens NX CAD/CAM software.

The AISI H13 steel was used as the workpiece material, and its chemical composition is presented in Table 1. The first machining experiments were conducted with the material in the annealed condition, with a hardness of 227 HV. The second batch of experiments was conducted with the material heat-treated to reach 495 HV (118% higher). To achieve this hardness, the procedure involved preheating at 816 °C (ramp rate of 10 °C/min), annealing at 600 °C for one hour in an argon atmosphere, followed by oil quenching (cooling rate of ~40 °C/min). Eight specimens were prepared for each machining condition, all prepared from the same batch.

To investigate the influences of the tool diameter, the experiments were conducted using two diameters of the ball-end mills: 10 mm and 6 mm. The cutting-edge roundness values were 5.6±0.76 µm and 2.7±0.60 µm, respectively, representing a proportional difference of approximately 22%. Both tools had a 30° helix angle and a multilayer (Al, Ti, Si, Cr)N coating. The cantilever ratio (L/D) was 4:1, and the tool run-out was 6.0±5 µm for the 6 mm tool and 12.0±8 µm for the 10 mm tool. The milling experiments were carried out on a Romi D600 CNC machining centre.

Based on the parameters recommended by the cutting tool supplier, the programmed cutting speed (Vc) was set to 150 m/min, and the radial depth of cut (ae) was fixed at 0.1 mm. Both parameters were kept constant. It is important to note that the effective cutting speed varied undesirably

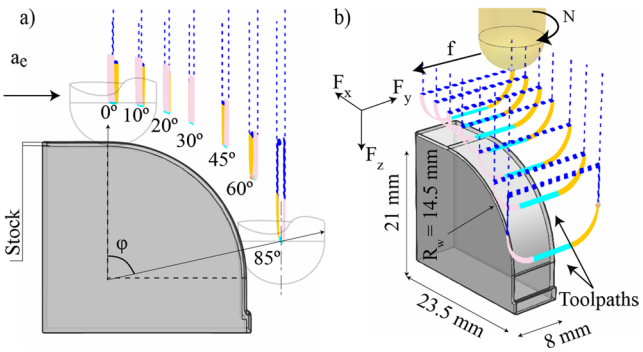

Fig. 1 Workpiece dimensions and cutting contacts evaluated

Table 1 Chemical composition of the AISI H13 provided by the supplier

Element	C	Si	Mn	Cr	Mo	V	Ni	Fe
% Weight	0.32–0.45	0.80–1.20	0.20–0.50	4.75–5.50	1.10–1.75	0.80–1.20	0–0.30.30	Balance

due to changes in tool–surface engagement. Two levels of axial depth of cut (ap: 0.5 mm and 0.2 mm) and feed per tooth (fz: 0.1 mm and 0.05 mm) were employed. It corresponds to 16 cutting parameter conditions (C1 to C16). Considering the seven contact angles (φ, Fig. 1), the experimental procedure carried out resulted in 112 milling experiments. The experimental matrix of the cutting parameters is presented in Table 2. For statistical purposes, ten tool passes were performed for each case.

It is important to highlight that this work focuses on understanding the influences of the material state and the cutting parameters a_p, f_z, tool diameter and the TSE when the ball-end mill tool tip is cutting.

The machining force was acquired by a Kistler® 9257BA dynamometer. A Kistler® 5233 A signal amplifier was used with a National Instruments USB-6216 data acquisition system, operating at a sampling rate of 100 kHz. Subsequently, the cutting force data were processed using Matlab® software, where the drift was removed, and the peak values of the Cartesian components of the machining force were obtained through the *findpeaks* function. Finally, the resultant cutting force was computed by pondering the local forces, as defined in Eq. 1.

$$F_u = \frac{1}{A}\sum_{i=1}^{A} F_u(i) \tag{1}$$

Table 2 Cutting parameters table

Workpiece	a_p [mm]	f_z [mm]	Tool diameter [mm]	ξ [°]	Material [Annealed/ Hardened]
C 1	0.5	0.10	10	22.4	H13 A
C 2	0.5	0.05	10	22.4	H13 A
C 3	0.2	0.10	10	14.1	H13 A
C 4	0.2	0.05	10	14.1	H13 A
C 5	0.5	0.10	6	30.7	H13 A
C 6	0.5	0.05	6	30.7	H13 A
C 7	0.2	0.10	6	19.2	H13 A
C 8	0.2	0.05	6	19.2	H13 A
C 9	0.5	0.10	10	22.4	H13 HT
C 10	0.5	0.05	10	22.4	H13 HT
C 11	0.2	0.10	10	14.1	H13 HT
C 12	0.2	0.05	10	14.1	H13 HT
C 13	0.5	0.10	6	30.7	H13 HT
C 14	0.5	0.05	6	30.7	H13 HT
C 15	0.2	0.10	6	19.2	H13 HT
C 16	0.2	0.05	6	19.2	H13 HT

Where F_u is the product of the force components x, y and z for each peak (Eq. 2).

$$F_u(i) = \sqrt{{F_x}^2{}_i + {F_y}^2{}_i + {F_z}^2{}_i} \tag{2}$$

The surface topography was assessed using a Veeco® WYKO NT1100® optical profilometer. For each sample, three random images were acquired at 10× magnification (736 × 480 µm), from which the surface texture and the Sz parameter were obtained after cylindricity removal using the F-operator and S-filtering (λs = 8 µm), following the procedure described by Pomberger et al. [30].

ANOVA analysis, under a 95% significance level, was performed to evaluate the significance of the cutting force and roughness, including interactions up to second order, aided by Minitab software.

2.2 Geometric identification tool-surface engagement

To support the analysis of the ball-end milling process, the tool–surface contacts were geometrically analysed, as shown in Fig. 2a. It illustrates the initial and final engagement of the tool edge with the workpiece surface, and the maximum and minimum effective cutting radius, which influence the effective cutting speed. The angle ξ is defined, and these conditions vary according to the contact angle (φ).

The geometric cutting conditions were obtained through parametric chip modelling in CAD software, with the cutting edge rotated in increments of 5° to represent the material removal process. Intermediate values were interpolated using Matlab® software, and the cutting contact area was determined by integrating the results over the tool inclination angles. A summary of this procedure is presented in Fig. 2b.

The effective cutting radii were calculated using Eq. 3 [22], with the minimum and maximum values determined by Eq. 4 and Eq. 5, respectively.

$$R_{ef} = \sqrt{R^2 - (R - a_p)^2} \tag{3}$$

$$R_{ef,min} = \bar{EC} = R\sin(\phi - \xi) \tag{4}$$

$$R_{ef,max} = \bar{AB} = R\sin(\phi) \tag{5}$$

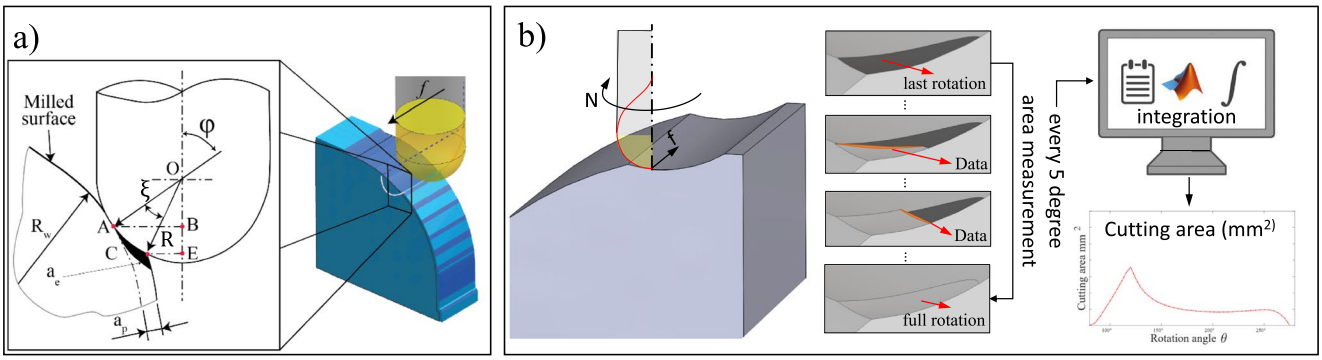

Fig. 2 **a** Tool surface engagement (TSE). **b** Obtaining the chip cross-sectional area

Where ϕ is the inclination angle, ξ is the chip extension angle, given by Eq. 6, as a function of the nominal tool radius (R), local radius of the surface (R_w), and depth of cut (a_p) [11].

$$\xi = \cos^{-1}\left[\frac{(Rw+R)^2+R^2-(Rw+a_p)^2}{2R(Rw+R)}\right] \quad (6)$$

For $\xi<\varphi$, the tool tip is out of contact (tip-off). For $\xi=\varphi$, the tool tip is on the surface (tip-on). For $\xi>\varphi$, the tool tip is engaged within the chip formation.

Finally, the effective cutting speed (Vc_{ef}) is obtained through Eq. 7.

$$Vc_{ef} = \frac{R_{ef}2\pi N}{1000} \quad (7)$$

3 Results and discussions

The results achieved in the research are presented, focusing on the influence of the material to be machined and the tool-surface engagement (TSE) to characterise the predominance of the cutting mechanism, from ploughing to shearing, which can influence the machining force (Fu) and the surface roughness when milling free-form surfaces using a ball-end cutting tool.

3.1 Machining force (Fu)

First, a general discussion about the resultant Fu of all experiments together with the ANOVA to identify the significance of each parameter evaluated on the Fu is introduced. After that, the influences of the cutting parameters (a_p and f_z) on the Fu, focusing on cases where the tool tip takes part in the cutting, were then investigated. The geometric characteristics were explored according to the TSE to aid the comprehension of the different behaviour of the machining force (Fu). Then, the Fu was decomposed to better understand the amount of ploughing and shearing mechanism according to TSE (φ and ξ). Finally, the computed K_s coefficients (specific pressure) are presented to estimate the Fu under such circumstances, ploughing and shearing.

3.1.1 Resultant Fu and its significant factors (ANOVA)

Figure 3 presents the average machining force (Fu) obtained from each experiment (C_x) for the seven TSE conditions evaluated (φ = 0° to 85°). Each set of experimental results is grouped according to similar parameters, where *An* denotes the annealed H13 and *Hd* represents its hardened H13 counterpart. The most important discussion about the results of Fu lies in two focuses: (i) the influences of the cutting parameters when the tool tip participates in the cutting process, and (ii) the influences of the material hardness in such a milling process. The contact angle φ (TSE) does not alter the chip cross-section thickness. From the contact angle φ = 45° onwards, the tool tip centre was no longer engaged in any condition, which may explain the lower average Fu values despite the material condition.

From the TSE point of view, the Fu increases drastically as the φ angle is reduced, for all cases. The increase of Fu can reach up to 400% from φ = 85° to 0° (C3 case). It happens because of the lower effective tool radius, thus lowering the effective cutting speed, as already documented in the current literature. However, unexpectedly, in some cases (for example, C1), where the tool tip is perpendicular to the machined surface (φ = 0°), the highest Fu was not observed. From the material point of view, unexpectedly, the hardened material had little influence on the Fu in most cases. To better understand such unexpected phenomena, the results of the ANOVA are first presented.

The ANOVA (Fig. 4) shows the significance of a_p, contact angle (TSE), f_z, and material hardness on the Fu, along with second-order interactions between contact angle and both a_p and f_z. For interpretation, factors with p-values below 0.05

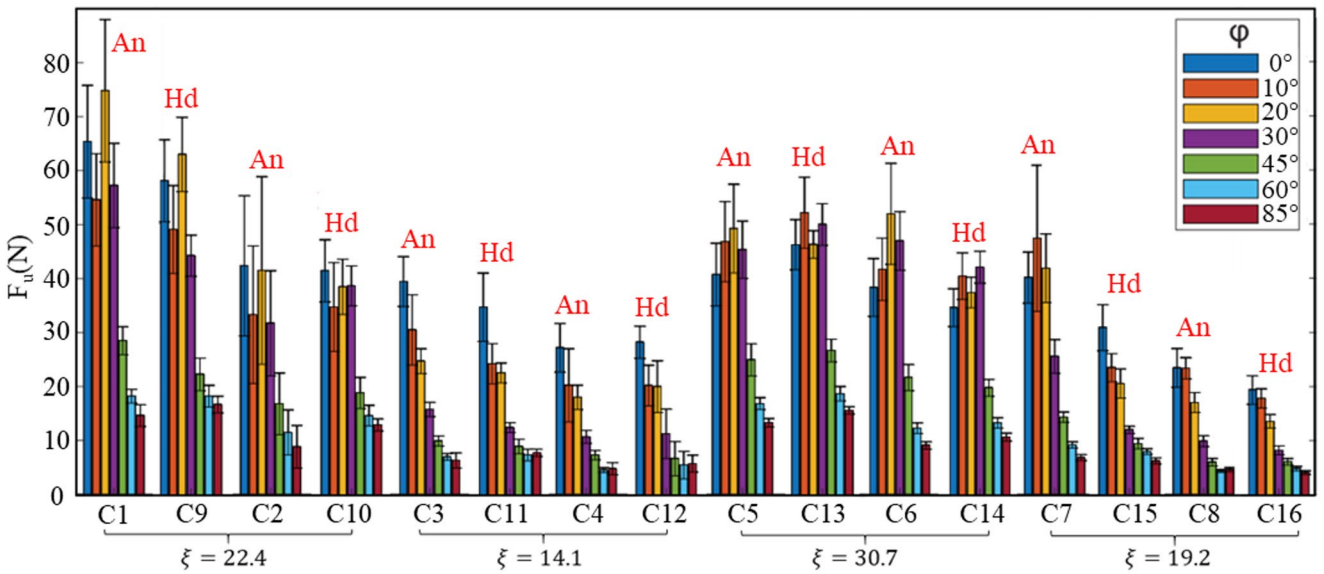

Fig. 3 The machining force for AISI H13 steel according to material hardness, cutting parameters and the TSE

Fig. 4 ANOVA results and main effect plot for the Fu

Source	DF	Seq. SS	Contribution	F-Value	P-Value
Contact angle	6	16591.6	50.89%	86.16	0.000
Material	1	181.0	0.56%	5.64	0.020
R	1	59.9	0.18%	1.87	0.175
a_p	1	8239.9	25.27%	256.75	0.000
f_z	1	2137.1	6.56%	66.59	0.000
Contact angle × a_p	6	1926.8	5.91%	10.01	0.000
Contact angle × f_z	6	609.8	1.87%	3.17	0.007
Error	89	2856.3	8.76%		
Total	111	32602.4	100.00%		

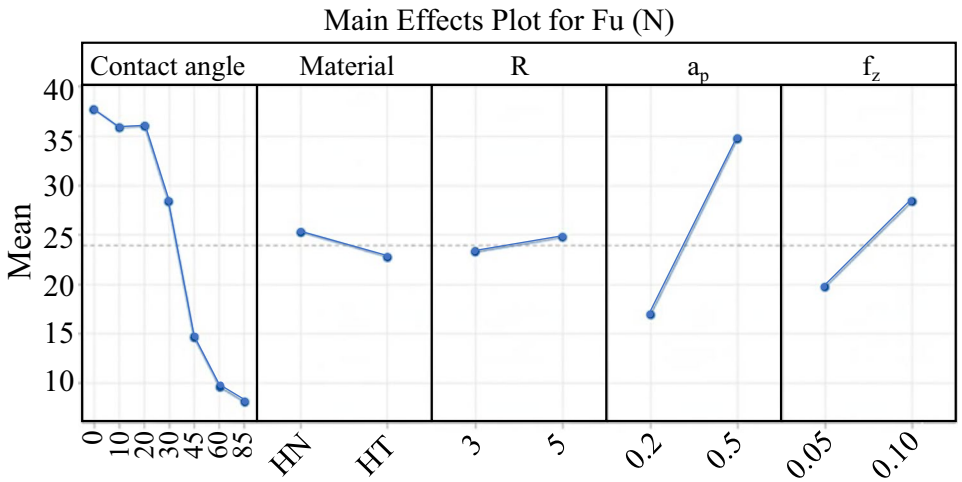

Table 3 Divergence of the Fu between the tool tip on and tool tip out according to a_p and f_z

	Fu (f_z)	
	f_z 0.05	f_z 0.1
Tool tip on cut (φ = 0° up to 30°)	30.7 N	44.8 N
Tool tip out of cut (φ = 85°)	6.3 N	9.2 N
Divergence of Fu: tip on and tip out	*385%*	*385%*
	Fu (a_p)	
	a_p0.2	**a_p0.5**
Tool tip on cut (φ = 0° up to 30°)	30.2 N	45.2 N
Tool tip out of cut (φ = 85°)	4.4 N	11.1 N
Divergence of Fu: tip on and tip out	*586%*	*307%*

are considered statistically significant, given the 95% confidence level assumed.

The ANOVA shows that the most significant contributions to the Fu are attributed to a_p, contact angle (φ), and f_z. The influences of the cutting parameters (a_p and f_z) on the Fu can be correlated to alterations of the chip cross-section, while the contact angle affects the tool tip engagement and modifies the cutting phenomena, such as the ploughing-to-shearing transition, which is one of the main aspects investigated in this work.

3.1.2 Influences of the cutting parameter ap and fz on Fu when the tool tip is on cutting

To understand the influences of the cutting parameters on the Fu and the influence when the tool tip takes part in the cutting process, the divergence of the Fu is compared between the cases in which the tool tip is engaged in cutting, compared to the cases in which the tool tip is out of cutting. The behaviour of this percentage divergence with respect to f_z and a_p is presented in Table 3.

Remarkably, Table 3 shows that the f_z does not affect the percentage divergence of the machining force (Fu) when the tool tip is on cut (tip-on) and the tool tip is out of cut (tip-out), across the different ranges of φ angle. It was kept the same (385%) for both values of f_z (0.05 mm and 0.1 mm). It probably happened because the f_z alters the chip by altering the tool surface contact in a radial direction, so the chip cross-section proportionally changes, and consequently, the region where ploughing and shearing occur. Besides, the cutting speed was the same for both f_z (Fig. 5a). Thus, the divergence of Fu between the tip-on and tip-out cutting conditions remains the same.

On the other hand, a_p had a significant influence on the Fu divergence with the tool tip actuation, in an inverse manner – the lower the a_p, the higher the percentage divergence. This probably occurs because a_p alters the chip volume in an axial direction and consequently, the proportion of the chips generated by ploughing remains the same when a_p is increased. Thus, the lower a_p, the higher percentage of the chip formed by the ploughing mechanism (see Fig. 5b). Besides, the effective tool radius is also altered, magnifying discrepancies. Consequently, because the ploughing mechanism requires a higher force to cut, in cases in which the ploughing volume is proportionally larger (relative to the shearing volume), the machining force would be higher as well.

The results show that for an accurate model to predict the machining force in such a milling process, the alterations of the parameter a_p significantly alter the Fu in tip-on cutting

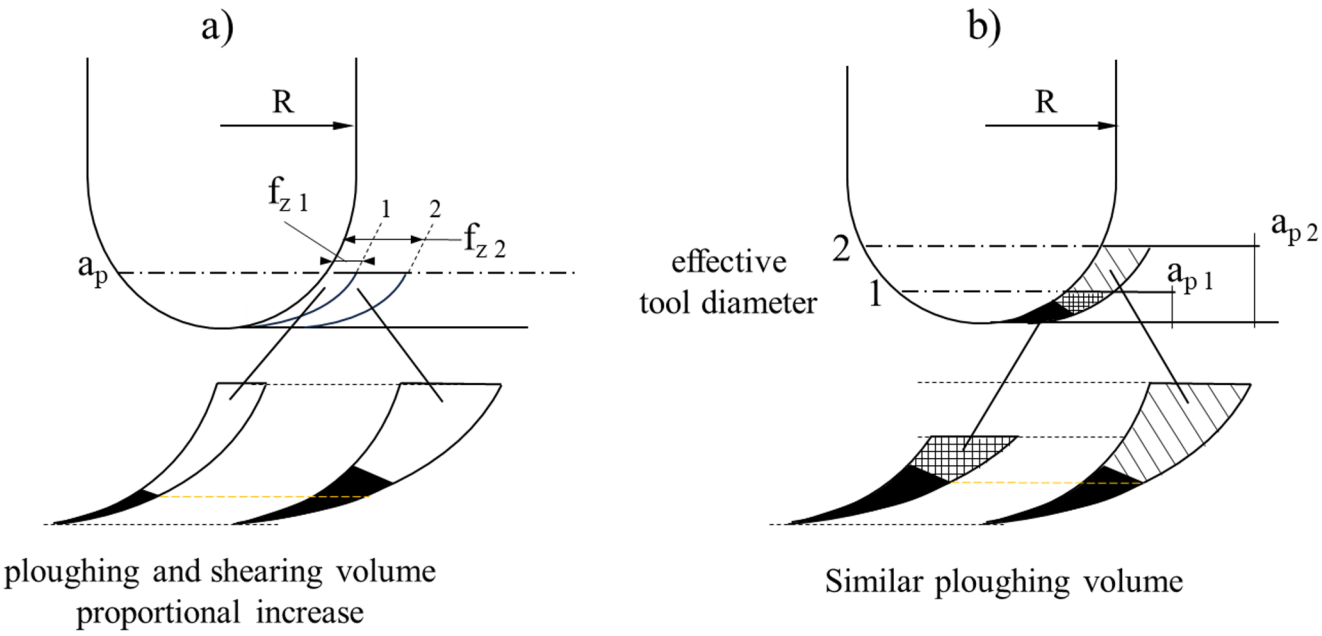

Fig. 5 Influences of the a_p and f_z on the effective tool diameter

conditions, and the alterations of the parameter f_z do not influence the divergence of the Fu between the tip-on and tip-out conditions. To better understand the cutting phenomena, the geometric variations of the TSE with tip-on and tool tip-out conditions are presented and discussed.

3.1.3 Geometric condition of the tool tip in the cutting zone

Another remarkable point observed in Fig. 3 is the unexpected behaviours of the Fu when the tool tip takes part in the cutting process. In some cutting conditions, when $\varphi = 0°$ (the tool tip perpendicular to the machined surface), the average Fu is not the highest value, as reported in the current literature. For example, in the case C5, the Fu was higher for $\varphi = 10°, 20°, 30°$ rather than for 0°. So, to understand such cases, a geometric evaluation is presented.

Figure 6 presents the engagement variation and the cutting speed limits for the different combinations of the cutting parameters investigated. It allows identifying that the tool surface engagement issue goes beyond the tool tip participating in the cutting process and the cutting speed variation. The angle ξ, which is a function of surface curvature radius, tool diameter and the depth of cut (Eq. 7), together with angle φ, defines the axial contact of the tool.

There is a range of positions in which the tool alters the axial quadrants of contact and can affect the cutting process. In some cases, the tool tip can act using two axial quadrants (Fig. 6b-ii). For any cutting parameters, when the angle φ is null Fig. 6b-i, only the tool's fourth axial quadrant (defined from the tool top view and the feed direction, counterclockwise) is in contact with the machined surface, whereas when $\varphi > \xi$, only the third axial quadrant of the tool is in contact with the machined surface (Fig. 6b-iv).

Therefore, this analysis allows the identification of four TSE conditions:

i) tool tip on cutting forming final surface ($\varphi = 0°$).
ii) tool tip on cutting with the cutting tool using two axial quadrants ($\varphi = \xi/2$).
iii) tool tip leaving the cutting zone ($\varphi = \xi$).
iv) tool tip is out of the cutting zone ($\varphi > \xi$).

Figure 6 demonstrates that for $\varphi = \xi/2$, the tool acts with half of the third and half of the fourth axial quadrants. By increasing the angle φ, the TSE passes through a transition phase, still in the tip-on cutting condition, increasing the effective cutting speed, until the tool tip leaves the cutting zone. After the tool crosses this transition zone, the chip is formed only using the fourth axial quadrant, with the tool tip out of the cutting zone. This results in a higher effective diameter and cutting speed, which leads to lower cutting forces as denoted in Fig. 3.

After this first geometric identification, the analysis of the chip formation according to the TSE angle is presented to aid the comprehension of the unexpected behaviours of the Fu and surface roughness. Figure 7 shows C7 as an example to illustrate the chip cross-sectional area and its position, where it occurs according to the tool rotation. Additionally, it shows the alteration of the axial quadrant ($\theta \approx 180°$) and the behaviour of the Cartesian components of the Fu, at $\varphi = 0°$, 10° and 20°.

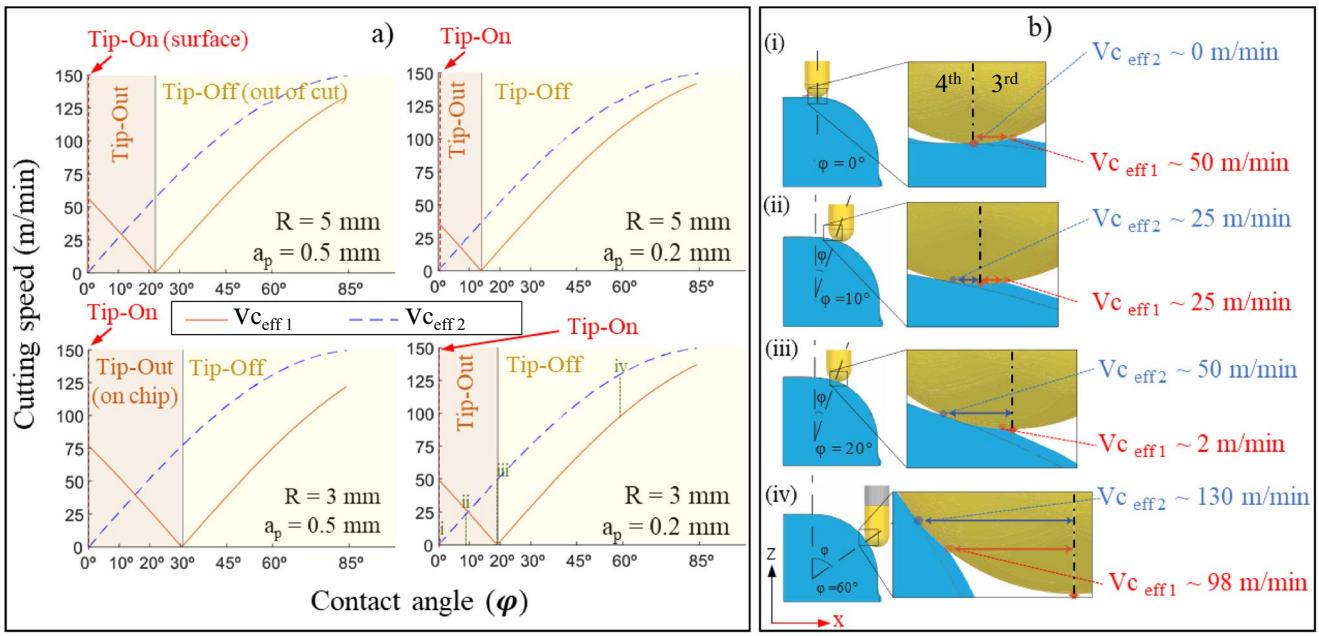

Fig. 6 Identification of tool surface engagement (TSE) according to ξ and φ

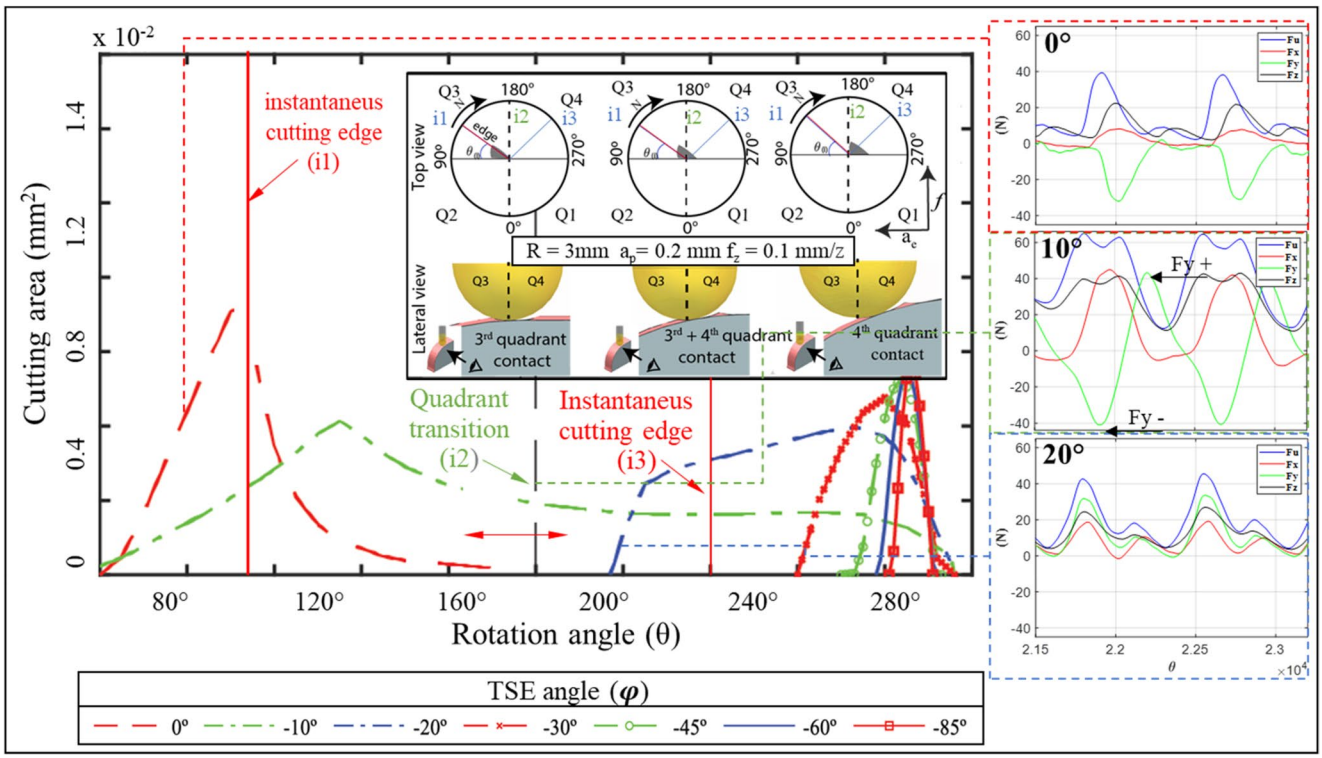

Fig. 7 Chip cross-sectional area at different inclination angles φ

Figure 7 shows that the chip is fully formed within the third axial quadrant when φ = 0°. For φ = 10°, an interesting point to be observed is that the chip formation alters between the third and fourth quadrants, which leads to the Cartesian component Fy of the machining force (Fu) altering its magnitude along one tool revolution (tooth pass), changing from −40 N to +40 N. The maximum divergence between +Fy and -Fy occurs about φ ≈ ξ/2. This condition contributes to plastic deformations such as ploughing. For the evaluated cutting condition (C16, ξ = 19.2°), when φ is higher than 20°, the chip is completely formed within the fourth axial quadrant.

Figure 8 presents the variation of the chip cross-section in relation to the average Fu for the cases investigated with a higher f_z level, 0.1 mm/z. The ξ and the Fu for each φ angle are correlated. Besides, it can be observed that a_p influences the cross-sectional area and, consequently, the axial quadrant transition, extending the effect to other TSE angles as a_p increases. The higher the ξ angle, the wider the transitional effect.

For the most stable behaviour of Fu, observed in cases C3 and C11 (Fig. 8c), the tool axial quadrant change occurs close to the machining experiment with φ = 10°, only observed in these cases. This narrow window for transition (low ξ) results in the force values behaving more consistently at low TSE angles; moreover, it exhibits a decreasing trend with increasing TSE angle, with Fu being highest at φ = 0° and decreasing until φ = 85°.

In contrast, Fig. 8b (ξ=30.7°) shows that higher ξ conditions increase the transition window, increasing the number of TSE angles that participate in the axial quadrant transition. This fact was responsible for an unexpected behaviour of Fu, where the highest Fu was not at φ = 0°, occurring under the tip-on cutting condition in the imminence of leaving the cutting zone (φ = 30°). After that, in the same cutting conditions, when φ = 45°, the chip is formed far from the tool axial quadrant transition zone, which resulted in a significantly lower Fu. Figure 8a shows a similar behaviour, with slightly more oscillations in Fu when the tool tip is under cutting, and ξ = 22° (intermediate value), depicting the influence of this transitory condition.

In general, the oscillation of the Fu observed in Fig. 3 at a lower value of φ (tool tip in cutting) can be associated with TSE conditions φ = 0°, φ = ξ/2, and φ = ξ, as well as material hardness. The results showed that a very complex cut phenomenon happens when the tool tip is in the cutting zone. The cases C7 and C15 were selected to demonstrate this complexity in the machining force (Fig. 8d).

Thereby, Fig. 9 presents this case in more detail. It shows that the chip formation at φ = 0°, 10°, and 20° is close to the tool axial quadrant transition zone. For the annealed material, the highest average of Fu did not happen at φ = 0°, as

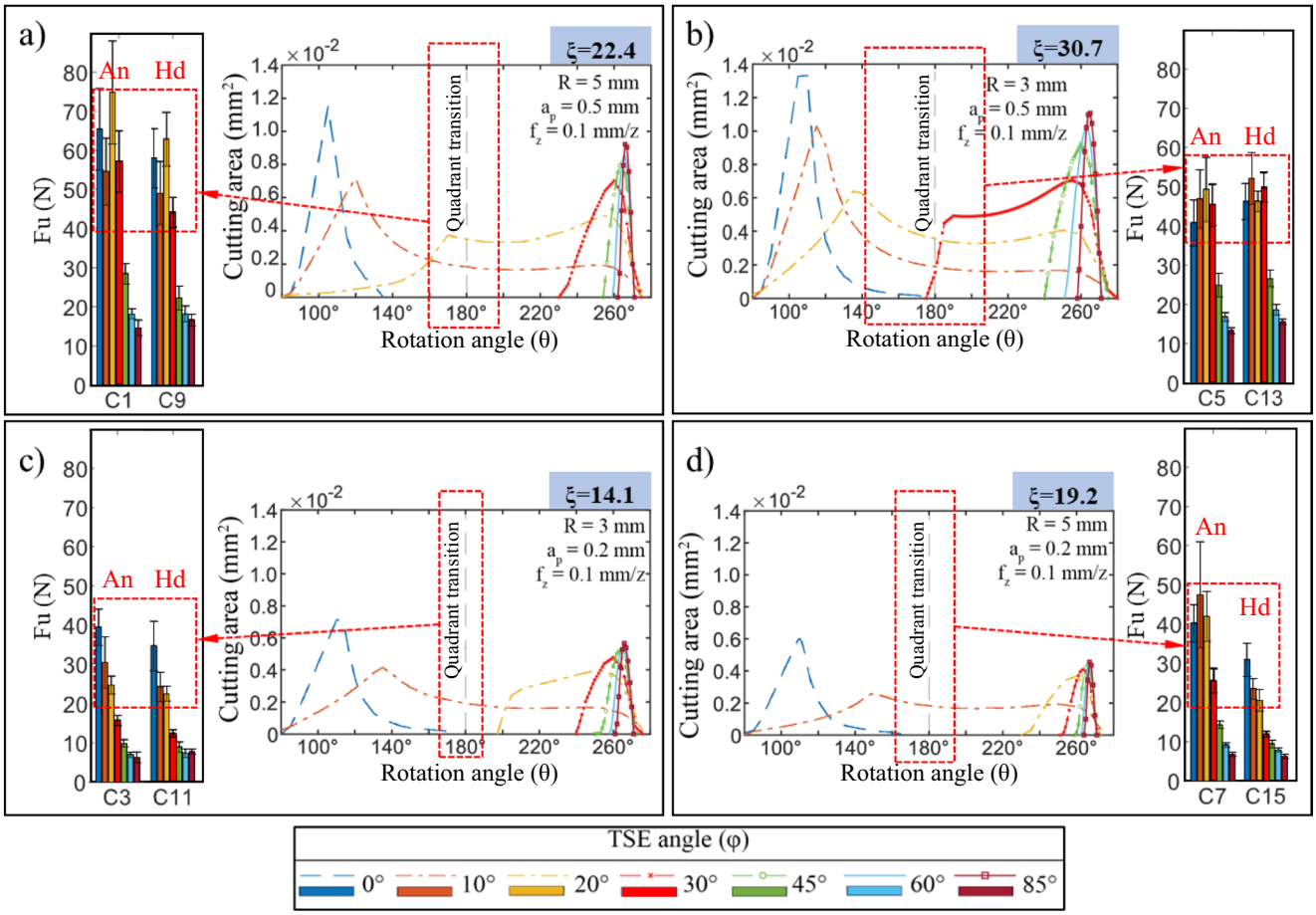

Fig. 8 Theoretical chip cross-section at different inclination angles φ and average Fu

previously documented in the current literature. The highest average of Fu occurred at φ = 10°, followed by φ = 20°. But for the hardened material, the Fu had an expected behaviour. It was higher at φ = 0° and it decreased significantly for higher φ values, almost in a linear way. Both cases (C7 and C15) are differentiated only by the hardness of the material.

Figure 9 shows a high discrepancy of Fu between the conditions in which the tool tip is in cutting (φ = 0°, 10°, 20°) and the conditions in which the tool is close to tangential milling (φ 85°). Besides, the Fu is much more influenced by the tool tip for milling the ductile material. Almost no discrepancy can be observed when tangential milling (φ = 85°). Thus, it can be concluded that the ploughing phenomenon plays a significant role in this process according to the material hardness state.

This probably happens because the increase in fragility with the hardness favours shearing, reduces the proportion of ploughing, particularly affecting the transition zone when the tool tip is in contact (φ = 0°, 10°, 20°). The highest average Fu did not occur at φ = 0°; it happened at φ = 10° and φ = 20°, which is close to ξ/2 (alteration of tool quadrant contact) and to φ ≈ ξ (tool tip leaving the cutting zone). On the other hand, in the case C15 (brittle material), the Fu had a behaviour already identified by the current literature, where the highest Fu occurred at φ = 0°, and it goes down close to a close-to-linear way. Therefore, for a future model to predict the Fu when the tool tip is on cut, a relationship among TSE angle (φ), ξ, and material hardness might be considered.

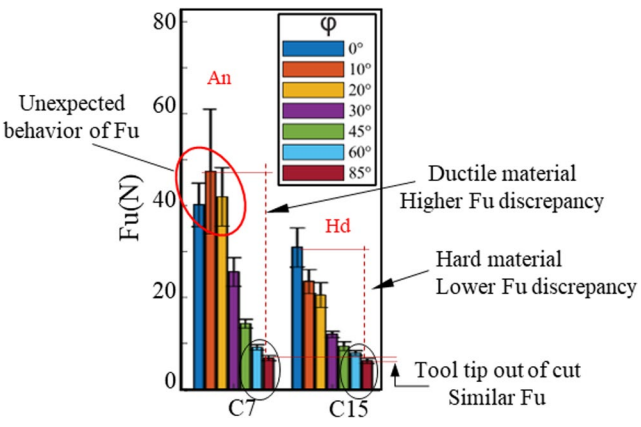

Fig. 9 Complexity of cutting involving TSE and material hardness

3.1.4 Components Fu ploughing (φ = tip on) and Fu shearing (φ = 85°) of the machining force

The current study opens a discussion on the quantification of the ploughing and/or shearing process of cutting when milling free-form shapes using a ball-end cutting tool. The increase in Fu when the tool tip acts in the cutting region probably occurs due to the lower cutting speed (close to zero at the tool tip), which promotes a predominant ploughing mechanism (associated with plastic deformation) instead of shearing, which would be preferable.

To aid the comprehension of the magnitude of the ploughing and/or shearing process under such milling conditions, the current paper proposes to split the Fu into two components when milling a free-form surface using a ball-end tool:

i) Fu_{shear}: the machining force necessary to cut the material, considering the shearing process. Currently, this is the only component considered to predict the Fu for ordinary milling (nominal tool diameter equal to effective diameter) using mechanistic models. Besides, in ordinary milling, shearing is the predominant cutting process.
ii) Fu_{plough}: the machining force necessary to smash the material during the cutting process, encompassing plastic deformations. Current models to predict this force have not been thoroughly discussed. It is likely to be more significant when machining ductile materials under low cutting speed and when a ball-end mill is used.

Thus, Fu is the resultant of both components (Eq. 8).

$$\mathrm{Fu} = \mathrm{Fu_{shear}} + \mathrm{Fu_{plough}}\,[\mathrm{N}] \tag{8}$$

It is known that for any cutting process, both shearing and ploughing happen. Shearing is predominant in tangential milling, with Fu_{plough} being neglected many times. However, in free-form milling, Fu_{plough} can be the greater component of the Fu. It is expected that a relationship exists between the material's ductility and the magnitudes of the two Fu components.

Unexpectedly, this paper shows that for the AISI H13, the annealed state (ductile) required a higher F_{plough} than the hardened state. The hardened H13 probably promotes more shearing, whereas in the annealed material, ploughing probably predominates. For the purpose of analysis, it is considered, by approximation, that at φ = 85° (tangential milling) only the shearing process happens, with Fu_{plough} neglected at this angle. So, at φ = 85°, the $Fu = Fu_{shear}$. When the tool tip is under cutting (φ = 0° up to 30°), $Fu = Fu_{shear} + Fu_{plough}$.

Based on that, Fig. 10 shows the average of Fu for all cases investigated in two circumstances: (i) Fu in tangential milling (φ = 85°), solid bars; (ii) Fu when the tool tip is engaged in the cutting (it can vary from φ = 0° to 30°, according to ξ), shown as hatched bars.

First, it can be observed that the Fu_{plough} component can reach up to 87% of the total Fu (tool tip on). Consider cases

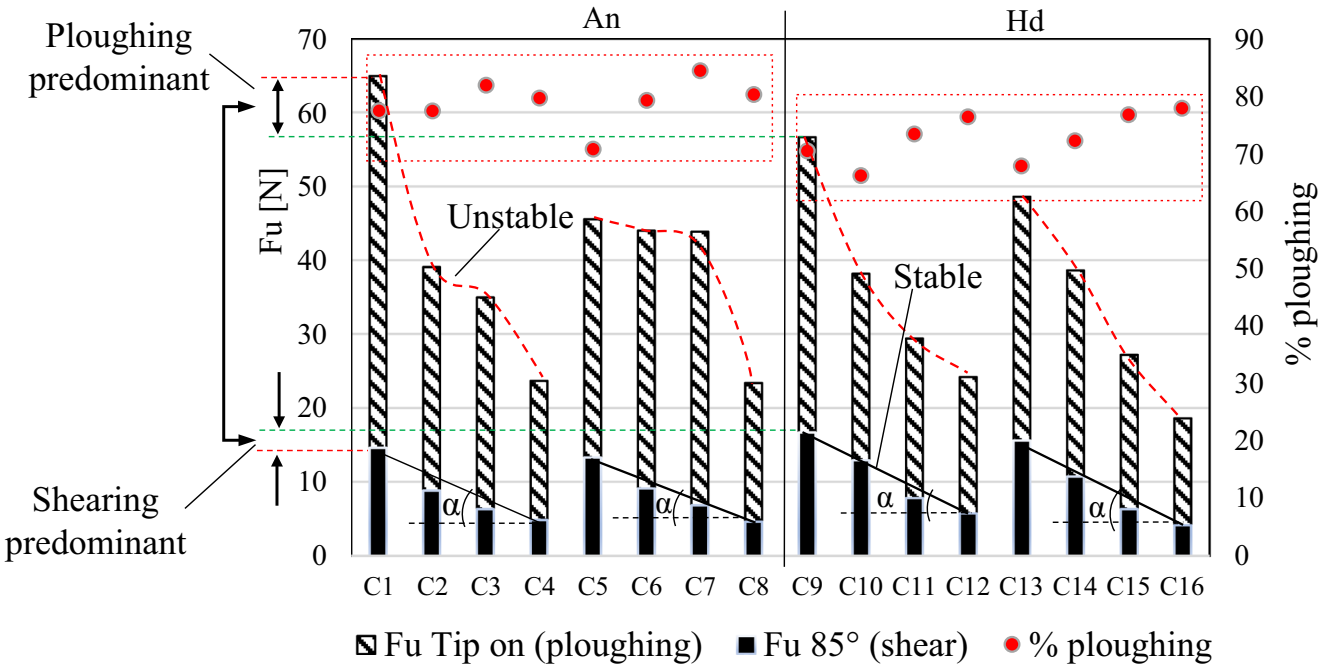

Fig. 10 Fu_{plough} and Fu_{shear} when the tool tip is engaged in the cut and the % ploughing

C1 (annealed) and C9 (hardened) to aid the discussion. At φ = 85° (solid bars), the hardened material requires a higher Fu than the annealed one. On the other hand, when the tool tip is on cutting, Fu is higher for the annealed material, increasing the % ploughing. In a simple view, it means that when the shearing is predominant (φ = 85°), the material hardness demands more Fu to be machined. However, when ploughing is predominant, the ductile material requires more Fu rather than the hardened material due to an increase in the Fu_{plough} component.

Another important observation in Fig. 10 is that at the shearing domain (φ = 85°), the behaviour of Fu more consistently follows the pattern of cutting parameter growth, in a very stable condition, illustrated by angle α. This contrasts with the behaviour of Fu when the tool tip is engaged in cutting. Based on these results, a new approach for specific pressure Ks is proposed, according to the TSE angle:

i) $Ks_{(\varphi)}$: machined regions where the tool tip is not engaged in cutting (φ > ξ); Fu can be estimated according to TSE.
ii) $Ks_{(\xi)}$: machined regions where the tool tip is engaged in cutting (φ < ξ); Fu might be driven by the three TSE condition identified before: (i) pure tool tip on cutting (φ = 0); (ii) cutting tool uses two axial quadrants (φ = ξ/2); and (iii) tool tip leaving the cutting zone (φ = ξ). Additionally, $Ks_{(\xi)}$ might also be related to the material hardness/ductility.

By using the conventional equation of Ks (Ks = F/A), Ks was plotted according to TSE (φ = 0° to 85°), which defines either $Ks_{(\varphi)}$ or $Ks_{(\xi)}$. Figure 11 shows Ks plots for the 10 mm diameter tool, encompassing the different materials and cutting parameters (for the tool of 6 mm in diameter, the behaviour was similar). For the TSE φ > ξ domain, the $Ks_{(\varphi)}$ follows a constant behaviour, and the graphics allow for

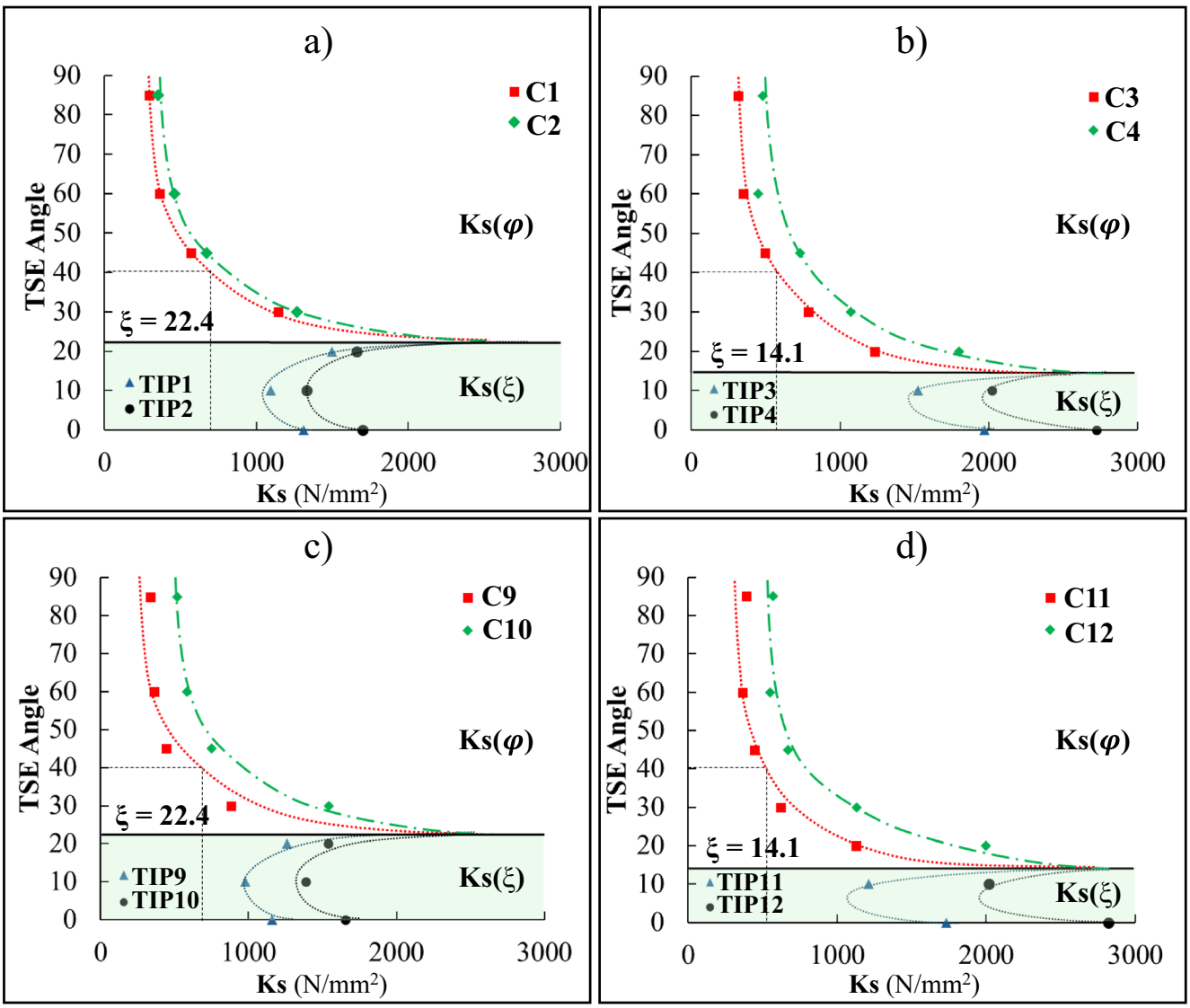

Fig. 11 Proposed Ks sub-domains: $Ks_{(\varphi)}$ and $Ks_{(\xi)}$

obtaining $Ks_{(\varphi)}$ according to TSE. However, for $Ks_{(\xi)}$, a non-constant behaviour is observed (following the Fu already discussed).

The results of this investigation show that $Ks_{(\xi)}$ cannot be established in a simple way. A small alteration of TSE (φ) can cause a large variation in Ks(ξ). Observing Fig. 10d, a variation of φ between 0° and 14° can alter about 50% the $Ks_{(\xi)}$. It is related to the TSE and its three regimes (φ = 0°, φ = ξ/2, φ = ξ) as well as the machined material properties. Thus, a better comprehension of $Ks_{(\xi)}$ is a suggestion to be investigated in future researches.

3.2 Roughness and surface texture

The results about the roughness of the machined surface focus on the influences of the tool surface engagement (φ and ξ), material hardness, and the cutting parameters to aid in the identification of the predominance of ploughing and/or shearing cutting mechanisms for milling free-form surfaces. Firstly, the overall roughness Sz and the significant effects of the parameters are presented and discussed. Later, the influence of Fu is correlated with the surface roughness.

Figure 12 presents the S_z values achieved in all experiments along with the standard deviation (three measurements for each condition). The hardened H13 produced lower Sz values on average with low standard deviation, in contrast to the annealed H13, which showed higher variability in Sz, which can be related to a higher level of plastic deformation.

This result shows that for the higher f_z (0.1 mm), the divergence between the roughness Sz is lower when the tool tip is cutting, φ = 0° and 10° (e.g., C1 and C9). When f_z is reduced (0.05 mm), the annealed H13 resulted in a significantly higher Sz than the H13 hardened. Probably it happens because reducing f_z reduces the chip cross section as well, and this fact, together with a more ductile material, increases the proportion of the ploughing process to remove material, which damages the surface roughness (Sz). To aid the comprehension of the roughness in this milling process, Fig. 13 presents the ANOVA analysis considering a confidence level of 95% together with the main effects plot for Sz.

The ANOVA indicates that, among the evaluated parameters, only the axial depth of cut (a_p) did not have a statistically significant effect on surface roughness. This is probably because increasing the axial depth of cut increases the chip volume mainly in the axial direction, while the volume of material removed that affects surface roughness is only slightly influenced. The most significant parameters affecting surface roughness follow the sequence: contact angle, tool radius, feed per tooth and the material state of the workpiece.

The dimensional cutting parameters (such as f_z, a_p, a_e and tool radius) influence the roughness predominantly from a geometric point of view. On the other hand, the material hardness and the cutting speed (altered by the TSE) can influence the roughness by altering the cutting mechanics (e.g., angle of the shearing plane, ploughing/shearing mechanism). Therefore, using only the values of Sz is not enough to know whether the roughness results from geometric conditions or from the mechanical cutting process itself. Then, the surface texture was examined to aid the discussion of the causes of the Sz value.

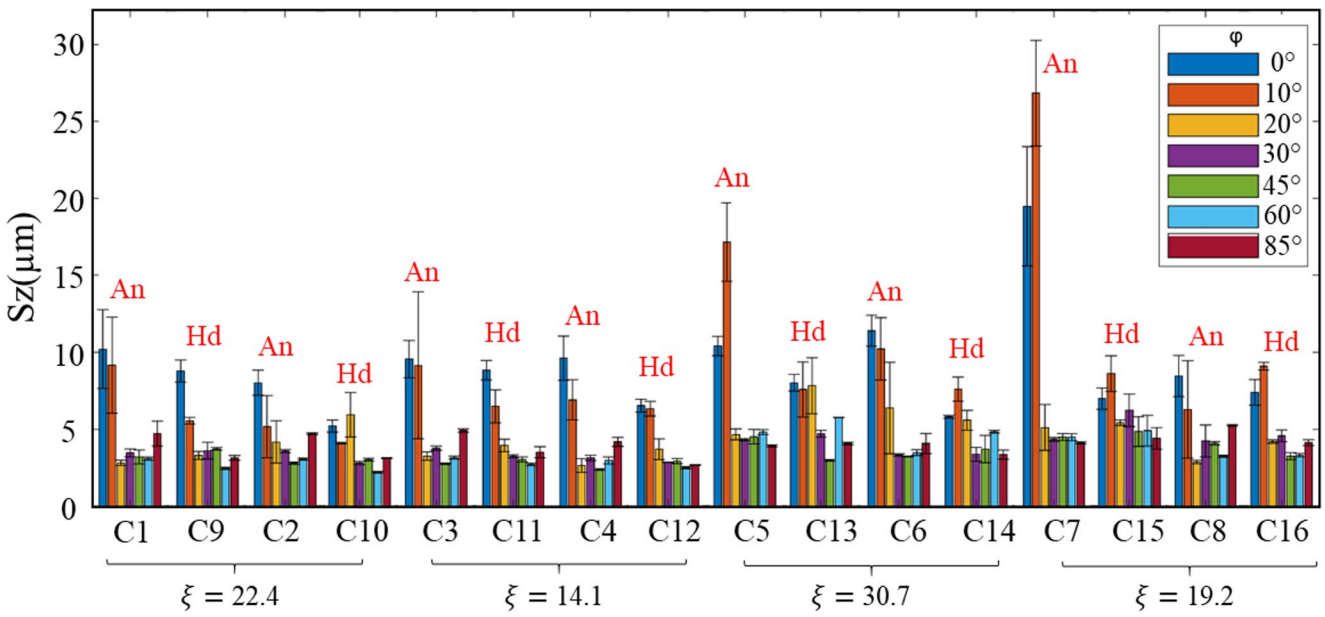

Fig. 12 Surface roughness according to contact angle under all cutting conditions

Source	DF	Seq SS	Contribution	F-Value	P-Value
Contact angle	6	635.15	47.55%	28.08	0.000
Material	1	35.23	2.64%	9.34	0.003
R	1	80.67	6.04%	21.40	0.000
a_p	1	2.31	0.17%	0.61	0.436
f_z	1	46.98	3.52%	12.46	0.001
Contact angle × Material	6	105.90	7.93%	4.68	0.000
Contact angle × R	6	57.80	4.33%	2.56	0.025
Contact angle × f_z	6	58.79	4.40%	2.60	0.023
Error	83	312.95	23.43%		
Total	111	1335.79	100.00%		

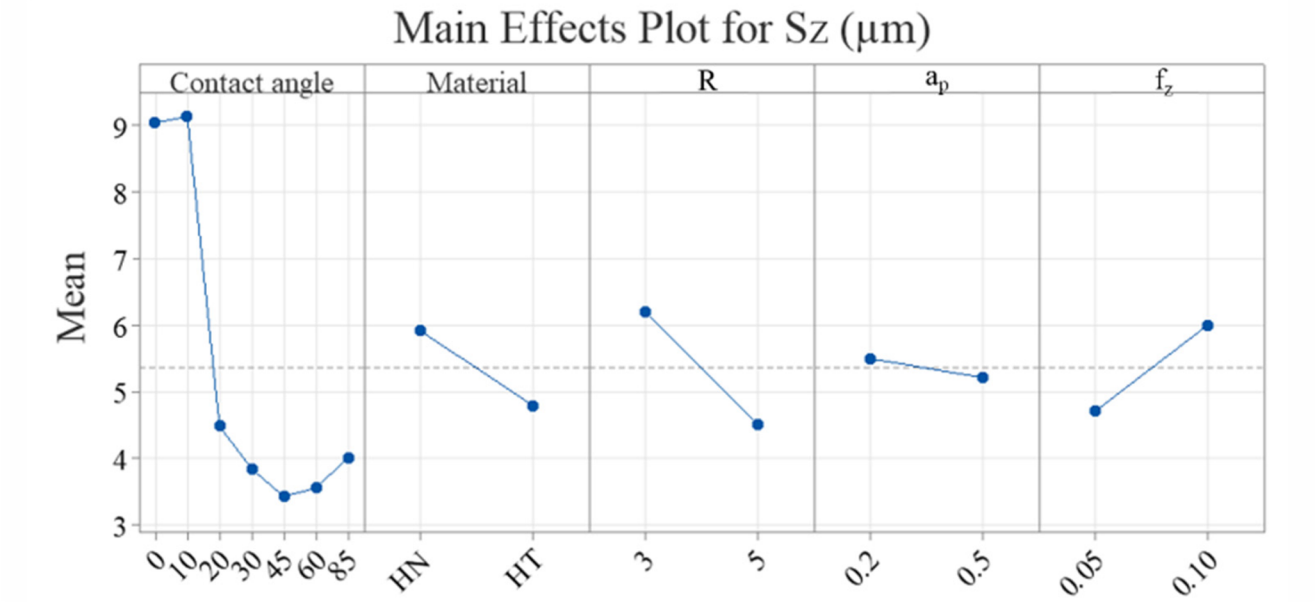

Fig. 13 ANOVA results in the average roughness (Sz) and its main effects

Figure 14 presents the surface texture obtained in cases of annealed H13 (cutting parameters C1, C2, C7) against its counterparts on hardened H13 (corresponding C9, C10, and C15) under the φ=0° condition (tool tip in contact with the final surface). First, it can be highlighted that for φ=0°, there is not a great discrepancy in the Sz values (Fig. 12) for annealed and hardened materials (except C7). It means that the tool tip severely influences the Sz, independent of the material hardness. But from the texture point of view, for the annealed H13, the value of the Sz is predominantly composed of material deformation rather than shearing cutting because the marks of tool action cannot be observed. In contrast, in the hardened H13 material, deformation can be observed together with the marks produced by the tool action, as the trocoidal movement of the tool and the f_z spacing.

Figure 14 allows the identification of some damages on the surface that influenced the Sz value when φ=0°: (i) scratches originated by ploughing, (ii) scratches originated by the cutting tool action.

As the tool tip moves away from the surface, the axial quadrant transition effect disappears, and the ploughing scratch marks are no longer observed. However, under this TSE condition, non-uniform burrs were produced when milling annealed H13, as shown in Fig. 15. Such burrs can be attributed to the ploughing phenomenon, induced by low cutting speed and high material ductility. This is not observed in the hardened H13. This phenomenon stops occurring at φ>ξ, where the tool tip is no longer in contact with the machined surface (Tip-off condition).

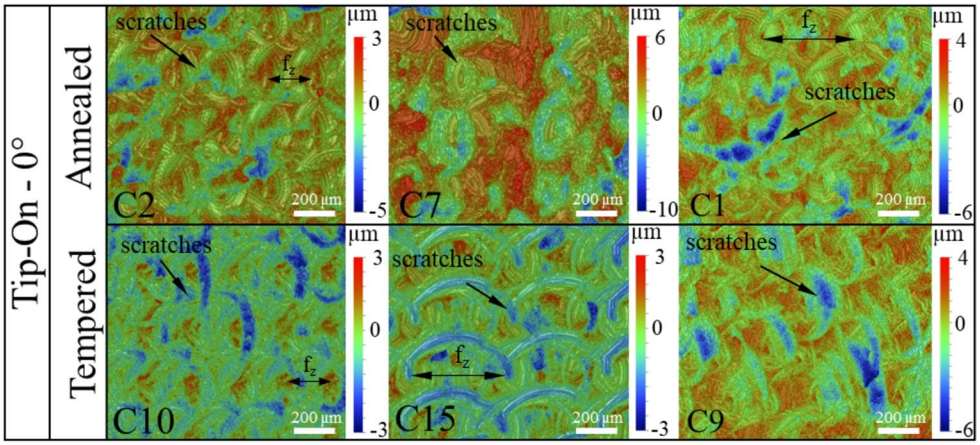

Fig. 14 Surface texture and damages for φ = 0°

Besides the geometric features (related to cutting parameters) that compose the Sz, the burr might also influence the Sz values for annealed H13.

For φ = 30°, 45° and 60°, the texture pattern does not alter significantly, with slight improvements up to φ = 85°. Then, the surface texture at φ = 85° is discussed, where the effective cutting speed is closer to the nominal one, favouring the shearing cutting. Figure 16 presents the results for annealed H13 (C1, C2, and C7) and hardened H13 (C9, C10, and C15). In this TSE, the ploughing scratches and burrs are not identified. This can be correlated with a higher cutting speed, which favours the shearing cutting mechanism, even for the annealed H13.

In the case of φ = 85°, the ploughing damages (scratches and burrs) are not identified. The surface texture is mainly influenced by the geometric condition of the cut (according to the cutting parameters) rather than material deformation. This effect is evident in both hardened and annealed materials.

Some longitudinal pattern texture can be identified in Fig. 16. At φ 85°, the axial component of the Fu (Fz) was significantly reduced, as illustrated by Fig. 17b (φ = 85°). Then, the main components of the Fu become Fx and Fy, which are responsible for deflecting the cutting tool, generating the form errors. According to Scandiffio et al. [26], the axial component of the Fu (Fz in this case) aids in reducing the tool deflection and it favours the cutting process stability. Therefore, longitudinal pattern deviation can be attributed to the relief of the axial component of Fu (Fz).

The texture presented in Fig. 17b and the Sz value (Fig. 12) show that the C7 condition presented the poorest surface roughness at φ = 10°. It can be explained by combining the factors: (i) critical TSE angle of φ ≈ ξ/2 (where ξ = 19.2°); (ii) critical cutting parameters for Sz as identified in the ANOVA; (iii) more ductile material (annealed H13); (iv) transition of the tool axial quadrant action during the chip formation (Fig. 7) that alters the direction of the Fy component of the Fu (Fig. 17b, φ = 10°). In these

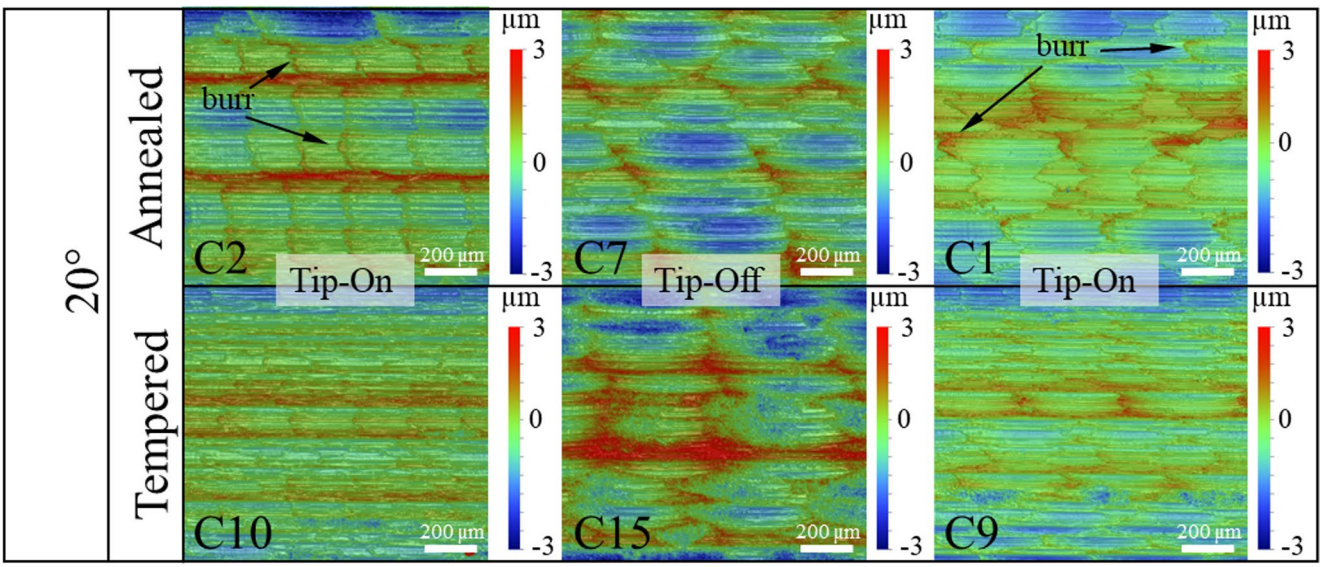

Fig. 15 Surface texture φ = 20°

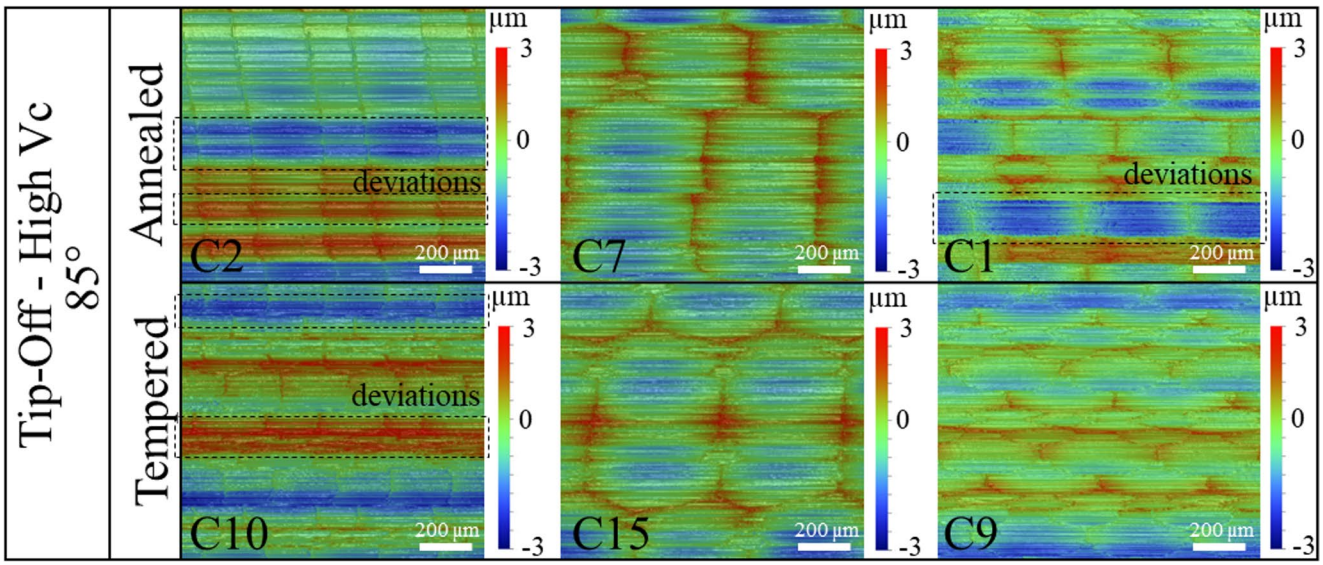

Fig. 16 Surface texture φ = 85°

circumstances, a higher deformation field occurred, generating another kind of surface damage by a ploughing-induced cavity, as identified in Fig. 17b (φ = 10°).

The surface texture images assessed in this research allowed the classification of five specific sorts of surface damage, focusing on the regions where the tool tip is engaged in or close to the cutting zone. These damages, depicted in Fig. 19, can be attributable to the ploughing/shearing cutting process, and they can influence the theoretical Sz values. The surface damages are:

i) *Predominant ploughing scratches*: At TSE φ = 0°, these are anomalous surface marks primarily generated by the displacement of material by either spare material (+) or unpattern removal (-) from the surface. It is promoted when the tool tip engages in cutting of ductile materials (annealed H13). The cutting tool marks are not distinctly visible in these instances (Fig. 18a).
ii) *Ploughing-induced deformations*: This type of damage was observed on annealed H13 surfaces at φ = 0°. It resulted from a volume of material being twisted at the same time that the tool tip centre scratches the surface (tool-on-surface interaction), deforming the surface with characteristic low elastic recovery, leading to detrimental surface roughness. This phenomenon was facilitated by the use of ductile materials combined with the influence of the tool tip, particularly at low cutting speeds, during the cutting process (Fig. 18a).
iii) *Predominant shearing scratches*: Even when the tool tip is engaged in cutting at lower speeds, hard materials (hardened H13) significantly promoted a material removal process primarily through shearing. This resulted in a clearly identifiable surface pattern produced by the cutting tool's action (Fig. 18b). This observation suggests that hardened H13 exhibited a greater tendency towards shearing, even at φ = 0° and 10°, whereas in annealed H13, ploughing was the more significant cutting mechanism.
iv) *Surface burrs*: This damage is observed during the milling of ductile material (annealed H13) across a range from φ = 20° to φ = 45°. In this scenario, the tool tip is on the verge of losing contact or no longer fully engaged in the main cutting zone. However, a lower effective tool radius and, consequently, lower effective cutting speeds contribute to the formation of surface burrs in ductile materials (Fig. 18c).
v) *Induced cavity formation*: Under specific TSE, the cutting edge operates within two axial quadrants, with the tool tip centre passing through at a certain instant. In these circumstances, during chip formation, the Cartesian components of the machining force (specifically Fy in this experimental setup) undergo a change in direction within a single chip formation cycle. This dynamic force alteration severely twists and plastically deforms the chip around the tool tip centre. The impact of this twisted chip against the machined surface can temporarily fuse the chip material onto the surface. Subsequently, due to the continuous twisting motion, a portion of the surface material fused with the chip is removed, thereby generating a surface cavity (Fig. 18d). This phenomenon was identified to occur when $\xi/3 < \varphi < \xi/2$ (in studied cases, it was identified at $\varphi \approx 10°$), becoming more pronounced as φ approaches ξ/2. Such damage was exclusively observed on annealed H13.

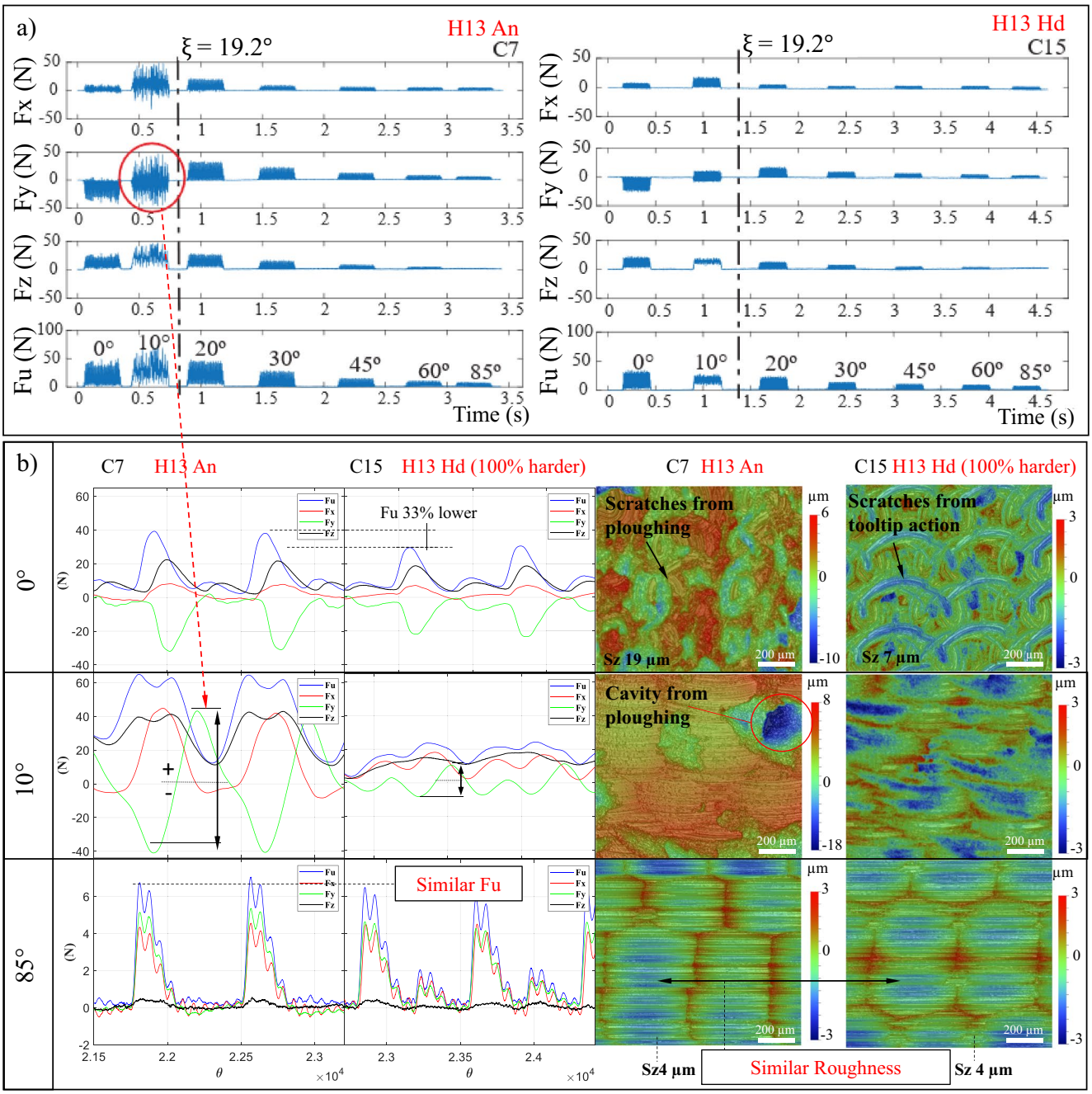

Fig. 17 Relationship between milling forces and surface texture under the most representative TSE conditions: φ = 0°, 10°, and 85°

After discussing the phenomena that occurred on the machined surface under the investigated cutting conditions, a Tukey analysis of the average surface roughness values was carried out along with the plotting of the average Sz by each parameter level (Fig. 19). It shows the surface roughness tends to remain similar between φ = 0° and φ = 10°.

Even though the material is not among the most significant contributions to the Fu and the S_z, the association of the material with the contact angle showed the most prominent second-order interaction to affect the machining process. The interaction between contact angle and feed per tooth (f_z) influenced the ploughing proportion by altering the chip formation according to the TSE.

4 Conclusions

The current research brings a contribution to the knowledge about milling of free-form surfaces using ball-end cutting tools towards a model to predict the machining force (Fu)

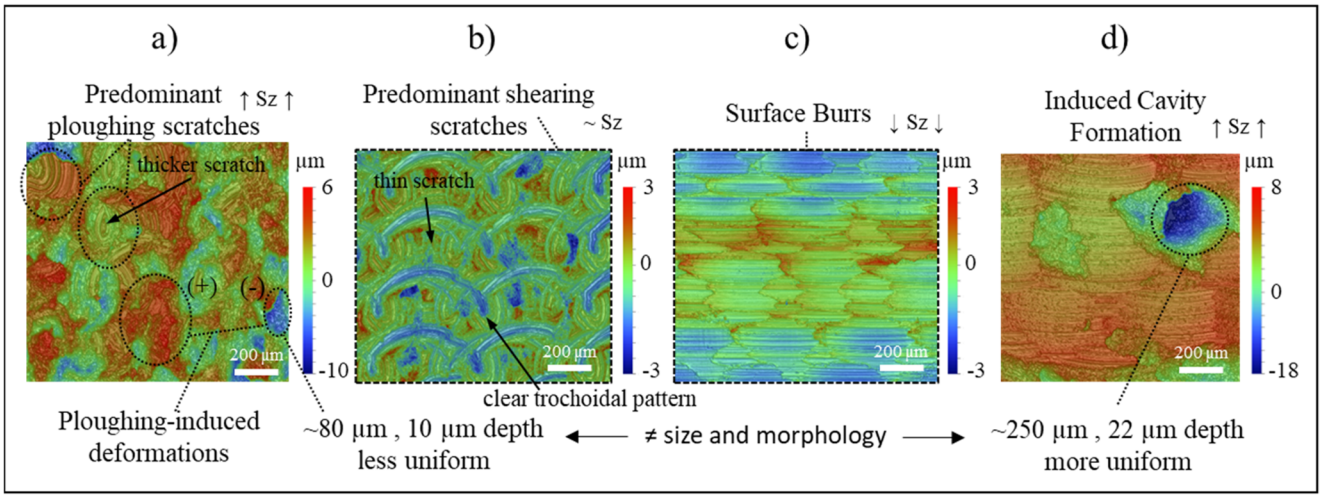

Fig. 18 Damage patterns attributable to the ploughing/shearing mechanism

and roughness (Sz) for this machining process. Milling experiments were conducted, and the influences of material hardness, cutting parameters, and the effects of tool surface engagement (TSE) were evaluated.

A determinant geometric cutting condition, the ξ angle, was identified by considering the cutting parameters and the TSE. The ξ angle enables determining the tool tip position and the chip engagement during the cutting process, which in turn affects the forces, surface texture, and consequently the roughness. Furthermore, it was observed that by altering the TSE and ξ angles, the transition between ploughing and shearing cutting mechanisms can be identified, along with a specific coefficient (Ks) defined according to the TSE and ξ angles: $Ks_{(\varphi)}$ and $Ks_{(\xi)}$. The definition of $Ks_{(\varphi)}$ and $Ks_{(\xi)}$ allowed identifying the machining force (Fu) to be determined at any specific position of the tool along a free-form path.

The main conclusions arising from this research are presented below. First, the conclusions about the TSE are presented, followed by the machining force (Fu), then the roughness (Sz and surface texture).

4.1 Tool surface engagement (TSE)

The geometrical analysis of the TSE (according to the tool position angle φ) allowed the identification of specific TSE conditions, to cite:

i) Tool tip on cutting against the machined surface (φ = 0°). This occurs when the tool axis is perpendicular to the machined surface normal and the cutting-edge acts using only one axial quadrant of the tool.
ii) Tool tip on cutting with the tool edge acting through two axial quadrants (φ = ξ/2).
iii) Tool tip at the point of leaving the cutting zone (φ = ξ).
iv) Tool tip out of the cutting zone (φ > ξ), increasing the effective cutting speed as the TSE angle increases.

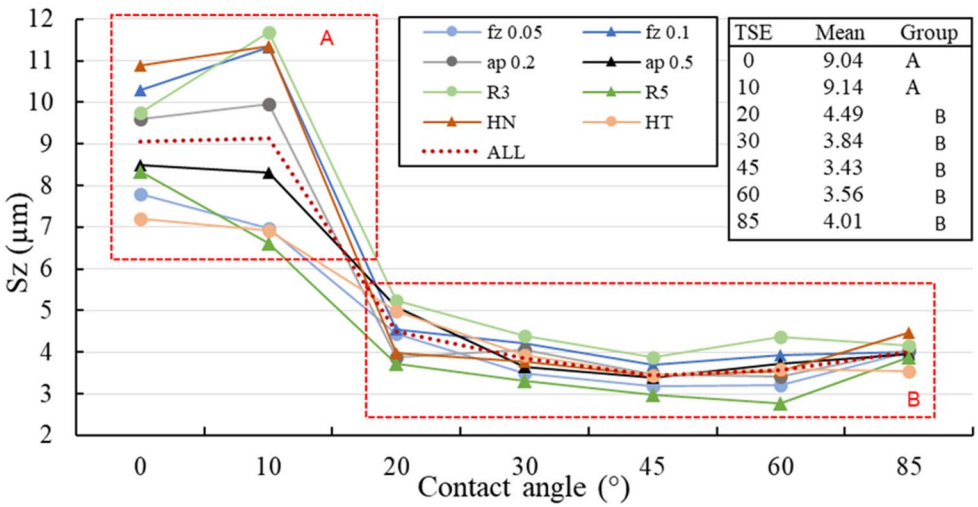

Fig. 19 Tukey analysis of average Sz values

4.2 Machining force (Fu) and Ks: $Ks_{(\varphi)}$ and $Ks_{(\xi)}$

- Contrary to previous studies, this research showed that the highest Fu did not occur at φ = 0° in most cases. Rather, the highest average Fu occurred around φ = ξ/2, where each tool edge cuts in two axial quadrants, altering the direction of the Cartesian component of Fu (Fy in this case), which in turn affects the surface texture.
- This research estimated the percentage of the shearing and/or ploughing process that comprises the Fu. It shows that the cutting parameter a_p does not influence the ploughing force component. Thus, to increase productivity, the a_p value can be raised without raising the ploughing force, avoiding its negative effects. Unlike f_z, the ploughing force increases proportionally with Fu when the f_z parameter.
- Annealed H13 steel required a higher machining force (Fu) than hardened H13 steel. Therefore, the ploughing component of the Fu is greater than the shearing component.
- At φ = 85°, a consistent shearing behaviour occurs, and the Fu follows linearly the alteration of the cutting parameters (angle α shown in Fig. 10). In contrast, at φ = 0°, where the tool tip is under cutting, no consistent behaviour was observed, and the ploughing component of the machining force reached up to 87% of the Fu.
- Evaluating the values of Fu, the TSE conditions (angles φ and ξ), the ploughing and shearing machining processes were identified, along with a new approach to defining Ks subdomains, to cite:
- - $Ks_{(\varphi)}$: machined regions where the tool tip is out of cutting (φ > ξ). It is a stable condition, and $Ks_{(\varphi)}$ is driven by the φ angle. The Fu can be estimated according to φ, as presented in Fig. 11.
- - Ks(ξ): machined regions where the tool tip is undercutting (φ < ξ). Fu is driven among three TSE conditions: (i) tool tip on cutting (φ = 0°); (ii) cutting tool uses two axial quadrants (φ = ξ/2); and (iii) tool tip at the point of leaving the cut (φ = ξ). It is not a stable condition due to the predominance of ploughing.

4.3 Roughness Sz and surface texture

- The results of the Tukey analysis for average roughness show a strong influence of the tool tip action at φ = 0° and φ = 10°, with a greater effect of the material state – the higher the hardness, the lower the roughness. For higher TSE angles (φ = 20° and beyond), neither material hardness nor the cutting parameters significantly affected the roughness.
- The surface texture images enabled the identification of five surface damage patterns related to the φ angle, material hardness and actuation of the axial quadrants, caused mainly by the ploughing effect during the cutting process, which influenced the Sz value. The five identified damage patterns are:

  i) Predominant ploughing scratches.
  ii) Predominant shearing scratches.
  iii) Ploughing induced deformations.
  iv) Surface burrs.
  v) Induced cavity formation.

To deepen the comprehension about this complex machining process towards an analytical model to predict it, the residual stress along with temperature, according to the tool-surface engagement is suggested to be investigated in future works.

Acknowledgements This research was partially funded by the National Council for Scientific and Technological Development (CNPq), under project 446919/2024-1, project 306438/2021-6, grant GD 140898/2023-9, and grant GDE 201478/2018-8, and by the Brazilian Federal Agency for Support and Evaluation of Graduate Education (CAPES).

Declarations

Competing interests All authors certify that they have no affiliations with or involvement in any organisation or entity with any financial interest or non-financial interest in the subject matter or materials discussed in this manuscript.
The authors declare no competing interests.
The authors declare that the paper is original and has been written based on the authors' own findings. All the figures and tables are original, and every expression from other published works was acknowledged and referenced. It is confirmed that all authors are aware of and satisfied with the authorship order and the correspondence of the paper.

References

1. Lasemi A, Xue D, Gu P (2010) Recent development in CNC machining of freeform surfaces: A state-of-the-art review. CAD Comput Aided Des 42:641–654. https://doi.org/10.1016/j.cad.2010.04.002
2. Tsai CL, Liao YS (2010) Cutting force prediction in ball-end milling with inclined feed by means of geometrical analysis. Int J Adv Manuf Technol 46:529–541. https://doi.org/10.1007/S00170-009-2155-Z/METRICS
3. Wang P, Zhang S, Yan ZG (2017) Study on surface defects in five-axis ball-end milling of tool steel. Int J Adv Manuf Technol 89:599–609. https://doi.org/10.1007/s00170-016-9113-3
4. Qin P, Wang M, Sun L (2020) Feed Rate Variation Strategy for Semi-Conical Shell Workpiece in Ball Head End Milling Process. Appl Sci 10:9135. https://doi.org/10.3390/APP10249135
5. Mali RA, Gupta TVK, Ramkumar J (2021) A comprehensive review of free-form surface milling– advances over a decade. J

Manuf Process 62:132–167. https://doi.org/10.1016/J.JMAPRO.2020.12.014
6. Basso I, Voigt R, Rodrigues AR et al (2022) Influences of the workpiece material and the tool-surface engagement (TSE) on surface finishing when ball-end milling. J Manuf Process 75:219–231. https://doi.org/10.1016/J.JMAPRO.2021.12.059
7. Li J, Kilic ZM, Altintas Y (2020) General cutting dynamics model for Five-Axis Ball-End milling operations. J Manuf Sci Eng Trans ASME. https://doi.org/10.1115/1.4047625/1084879. 142:
8. Varghese A, Kulkarni V, Joshi SS (2021) Monitoring shearing-plowing transitions in micro-milling using fluctuations in cutting forces. J Micro Nanomanuf 9. https://doi.org/10.1115/1.4053696/1133357
9. Feng Y, Hung TP, Lu YT et al (2019) Surface roughness modeling in Laser-assisted end milling of inconel 718. Mach Sci Technol 23:650–668. https://doi.org/10.1080/10910344.2019.1575407
10. Pan Z, Feng Y, Lu YT et al (2017) Force modeling of inconel 718 laser-assisted end milling under recrystallization effects. Int J Adv Manuf Technol 2017 92(5):2965–2974. https://doi.org/10.1007/S00170-017-0379-X
11. Marin F, Fagali de Souza A, da Silva Gaspar H et al (2024) Topography simulation of free-form surface ball-end milling through partial discretization of linearised toolpaths. Eng Sci Technol Int J 55:101757. https://doi.org/10.1016/J.JESTCH.2024.101757
12. Souza AF, De, Machado A, Beckert SF, Diniz AE (2014) Evaluating the roughness according to the tool path strategy when milling free form surfaces for mold application. Procedia CIRP 14:188–193. https://doi.org/10.1016/J.PROCIR.2014.03.089
13. de Lacalle LN, Lamikiz A, Sánchez JA, Salgado MA (2007) Toolpath selection based on the minimum Deflection cutting forces in the programming of complex surfaces milling. Int J Mach Tools Manuf 47:388–400. https://doi.org/10.1016/j.ijmachtools.2006.03.010
14. Arrizubieta JI, Cortina M, Mendioroz A et al (2020) Thermal diffusivity measurement of laser-deposited AISI H13 tool steel and impact on cooling performance of hot Stamping tools. Met (Basel) 10. https://doi.org/10.3390/met10010154
15. Mazur M, Leary M, McMillan M et al (2016) SLM additive manufacture of H13 tool steel with conformal cooling and structural lattices. Rapid Prototyp J 22:504–518. https://doi.org/10.1108/RPJ-06-2014-0075
16. Wang JJJ, Zheng MY (2003) On the machining characteristics of H13 tool steel in different hardness States in ball end milling. Int J Adv Manuf Technol 22:855–863. https://doi.org/10.1007/s00170-003-1663-5
17. de Lacalle LNL, Lamikiz A, Sánchez JA, Salgado MA (2004) Effects of tool Deflection in the high-speed milling of inclined surfaces. Int J Adv Manuf Technol 24:621–631. https://doi.org/10.1007/s00170-003-1723-x
18. Shtehin OO, Wagner V, Seguy S et al (2017) Stability of ball-end milling on warped surface: semi-analytical and experimental analysis. Int J Adv Manuf Technol 89:2557–2569. https://doi.org/10.1007/s00170-016-9656-3
19. Ozturk E, Budak E (2007) Modeling of 5-axis milling processes. Mach Sci Technol 11:287–311. https://doi.org/10.1080/10910340701554808
20. Wojciechowski S, Maruda RW, Barrans S et al (2017) Optimisation of machining parameters during ball end milling of hardened steel with various surface inclinations. Meas (Lond) 111:18–28. https://doi.org/10.1016/j.measurement.2017.07.020
21. Wojciechowski S, Krajewska-Śpiewak J, Maruda RW et al (2023) Study on ploughing phenomena in tool flank face – workpiece interface including tool wear effect during ball-end milling. Tribol Int 181:108313. https://doi.org/10.1016/j.triboint.2023.108313
22. de Souza AF, Diniz AE, Rodrigues AR, Coelho RT (2014) Investigating the cutting phenomena in free-form milling using a ball-end cutting tool for die and mold manufacturing. Int J Adv Manuf Technol 71:1565–1577. https://doi.org/10.1007/s00170-013-5579-4
23. García-Barbosa JA, Arroyo-Osorio JM, Córdoba-Nieto E (2017) Influence of tool inclination on chip formation process and roughness response in ball-end milling of freeform surfaces on Ti-6Al-4V alloy. Mach Sci Technol 21:121–135. https://doi.org/10.1080/10910344.2016.1260434
24. Yao C, Tan L, Yang P, Zhang D (2018) Effects of tool orientation and surface curvature on surface integrity in ball end milling of TC17. Int J Adv Manuf Technol 94:1699–1710. https://doi.org/10.1007/s00170-017-0523-7
25. Wu S, Yang L, Liu X, li et al (2017) Effects of curvature characteristics of sculptured surface on chatter stability for die milling. Int J Adv Manuf Technol 89:2649–2662. https://doi.org/10.1007/s00170-016-9560-x
26. Scandiffio I, Diniz AE, de Souza AF (2016) Evaluating surface roughness, tool life, and machining force when milling free-form shapes on hardened AISI D6 steel. Int J Adv Manuf Technol 82:2075–2086. https://doi.org/10.1007/s00170-015-7525-0
27. Magalhães LC, Ferreira JCE, de Castro Bezerra AL, Sombra SC (2019) Influence of feed direction on finishing milling cylindrical surfaces in H13 hardened steel. J Brazilian Soc Mech Sci Eng 41:1–8. https://doi.org/10.1007/s40430-019-1668-0
28. de Souza AF, Berkenbrock E, Diniz AE, Rodrigues AR (2015) Influences of the tool path strategy on the machining force when milling free form geometries with a ball-end cutting tool. J Brazilian Soc Mech Sci Eng 37:675–687. https://doi.org/10.1007/s40430-014-0200-9
29. Soori M, Arezoo B, Habibi M (2014) Virtual machining considering dimensional, geometrical and tool Deflection errors in three-axis CNC milling machines. J Manuf Syst 33:498–507. https://doi.org/10.1016/j.jmsy.2014.04.007
30. Pomberger S, Stoschka M, Leitner M (2019) Cast surface texture characterisation via areal roughness. Precis Eng 60:465–481. https://doi.org/10.1016/j.precisioneng.2019.09.007